

Is nanostructuring sufficient to get catalytically active Au?

Alexander Yu. Klyushin^{1,2}, Mark T. Greiner¹, Xing Huang¹, Thomas Lunkenbein¹, Xuan Li¹,
Olaf Timpe¹, Matthias Friedrich¹, Michael Hävecker³, Axel Knop-Gericke¹ and Robert
Schlögl^{1,2,3}.*

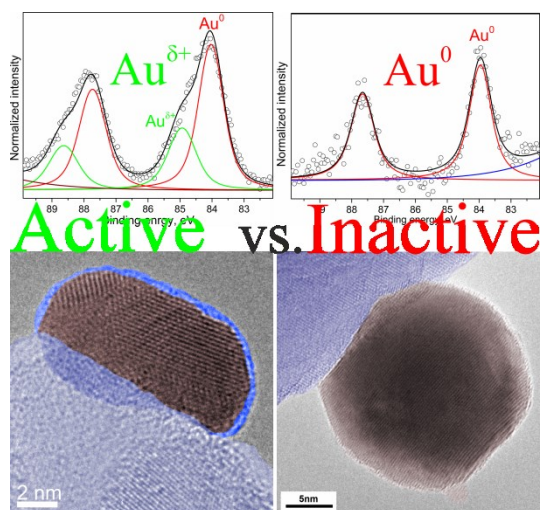
¹ Fritz-Haber-Institut der Max-Planck-Gesellschaft, Faradayweg 4-6, 14195 Berlin, Germany.

² Division Energy Material, Helmholtz-Zentrum Berlin für Materialien und Energie GmbH,
Albert-Einstein-Str. 15, 12489 Berlin, Germany.

³ Department of Heterogeneous Reactions, Max-Planck-Institut für Chemische
Energiekonversion, Stiftstrasse 34 – 36, 45470 Mülheim an der Ruhr, Germany.

Gold nanoparticles on transition metal oxides were synthesized by two different methods: precipitation and photo-induced decomposition of intermediate gold-azido complex. Only samples prepared by precipitation method showed significant CO conversion at low temperature. XPS shows the formation of two Au species (Au^0 and $\text{Au}^{\delta+}$) on the surface of active Au/TiO₂ and Au/Fe₂O₃ samples. The energy shift of $\text{Au}^{\delta+}$ peak depends on the support and is 0.6 eV and 0.9 eV for Au/TiO₂ and Au/Fe₂O₃, respectively. TEM images indicate the formation of overlayer on Au particles. These results prove Au activation via a Strong Metal Support Interaction, based on

strong influence of the support on the electronic structure of the gold through charge transfer and stabilization of low-coordinated Au atoms.



Keywords: Gold nanoparticles, $Au^{\delta+}$, X-ray photoemission spectra, transmission electron microscopy, CO oxidation, strong metal-support interaction.

1. INTRODUCTION

Due to its inert nature, gold has traditionally been ignored for catalytic purposes. However, ever since the discovery of catalytically active gold nanoparticles (Au NPs) supported on metal oxides by Haruta et al.¹, Au-based catalysts have attracted a lot of attention from the scientific community. It is generally acknowledged that the catalytic behavior of extended Au surfaces is vastly different from that of supported nanoscopic Au, but the nature of the active sites on gold is still a matter of active debate in the literature.² Numerous studies of the underlying physical phenomena have come to partly contradictory conclusions.^{3,4} One of the more common conclusions is that the way in which gold acts catalytically is substantially different from the other metals of the platinum group.⁵

Previously we concluded that Au NPs are not active in CO oxidation when supported on oxygen-free supports—such as Au foil, highly oriented pyrolytic graphite (HOPG), O- and N-functionalized carbon nanotubes (O-CNTs and N-CNTs).⁶ Several studies of Au NPs on oxide supports—such as CeO₂⁷, TiO₂⁸, Fe₂O₃⁹, FeO¹⁰—revealed that some of the common factors affecting catalytic behavior are particle size¹¹, method of preparation¹², pretreatment¹³, oxidation state of Au¹⁴. However, the role of the support for the catalytic reaction is still under debate, and the identification of the nature of the active sites requires a systematic study of Au-based catalysts.

Here, we present a study of Au catalysts on transition metal oxides, which were synthesized by photo-induced decomposition of Au-azido-complex (Au/Fe₂O₃-PC) and precipitation (Au/Fe₂O₃-C, Au/TiO₂-DP) methods, in the CO oxidation reaction, using a combination of near-ambient-pressure XPS (NAP-XPS), transmission electron microscopy (TEM) and electron-energy-loss spectroscopy (EELS). NAP-XPS measurements allow an *in-situ* characterization of the electronic structure of nanoscopic Au and its support, while electron microscopy provides information about the morphology of Au NPs before and after reaction. In addition, the EELS technique provides microscopic chemical information of the Au NPs' local environment. The combination of these techniques helps to understand the nature of active site of Au and clarify the mechanism of the reaction.

2. METHODS

2.1 XPS

The experiments were performed at the ISSS beamline of BESSY II/HZB (Berlin, Germany). All measurements were carried out in a stainless steel NAP-XPS chamber described in detail

elsewhere.¹⁵ The powder samples were pressed together with a copper mesh into a pellet of 8 mm diameter. The copper mesh was used to prevent sample charging during photoemission. All samples were mounted on a sapphire sample holder, between a stainless steel back-plate and a lid with a 6 mm hole. The samples were heated from the backside by an infrared laser, the temperature was measured by a thermocouple clamped to the sample's surface. The overall spectral resolution was 0.3 eV in O1s, 0.2 eV in Au4f regions. The core level binding energies (BE) were calibrated using the Au4f_{7/2} and C1s second-order peaks. The accuracy of BE calibration was estimated to be around 0.05 eV.

All XP spectra were collected in normal photoemission mode. For quantitative XPS analysis least-squares fitting of the spectra was performed using CasaXPS software. A Doniach-Sunjic and Gaussian-Lorentzian product line shapes were used to fit the Au4f_{7/2} and O1s, respectively. A Shirley-type background was subtracted before the spectra were fit.

O₂ and CO were dosed into the experimental cell, in various ratios, using mass-flow controllers at a sample temperature of 100 °C. The total pressure in the experimental cell was 0.3 mbar.

2.2 TEM and EELS

TEM images were recorded using a Cs-corrected (CEOS) FEI Titan 80-300 equipped with a Gatan Tridiem Image Filter and EELS spectra were measured using a Philips CEM 200 and a Cs-corrected (CEOS) FEI Titan 80-300 equipped with a Gatan Tridiem Image Filter. Spectra were acquired from different regions of the sample, using a dispersion of 0.3 eV as well 0.1 eV and an acquisition time of 10 s. The spectrometer entrance aperture was set to 2 mm and 1 mm, respectively.

2.3 CO oxidation at atmospheric pressure.

CO oxidation was investigated in a plug-flow fixed-bed reactor. Gases (He, H₂, O₂, CO) are mixed via custom-designed switching valves. The U-tube reactor (i.d. = 5mm) is made of glass lined steel and is connected to a four-way valve used as bypass. The reactor is heated by a copper block oven, providing an isothermal (± 1 °C) zone of 4 cm at temperatures up to 400 °C. The temperature is monitored inside the catalyst bed. Analytics are performed by an on-line detector consisting of IR detectors for CO, CO₂ and H₂O and a paramagnetic sensor for O₂ (X-Stream, Rosemount).

For the catalytic tests, 50 mg of the sample were diluted by 250 mg SiC. CO oxidation was investigated at room temperature (RT), 50 °C, 100 °C and 200 °C. The feed consisted of 1.0 mL/min CO and 2.0 mL/min O₂ balanced with 97 mL/min He. Oxidative treatment of the sample was carried out at 400 °C for 1 h in 20 mL/min O₂ and 80 mL/min He. Blank activity in the empty reactor is not detectable at temperatures below 200 °C.

3. RESULTS

3.1 Au/Fe₂O₃-PC.

3.1.1 TEM characterization.

In order to have a benchmark for comparison, the first step in this study was to characterize the morphology of freshly prepared catalysts. A TEM image of an untreated Au/Fe₂O₃-PC is presented in the Figure 1A. The image shows a round Au NP of about 20 nm in diameter (ESI, Figure S1). Because of the shape a complex faceting is there, the Au surface has a lot of steps and edges. The contact angle between the Au NP and Fe₂O₃ is high, no spreading of the support material over the Au NP surface was observed. Subsequent exposure to CO:O₂=1:2 at 300 °C

does not change Au NPs significantly, retaining the same mean particle size as before oxidation (Figure 1B).

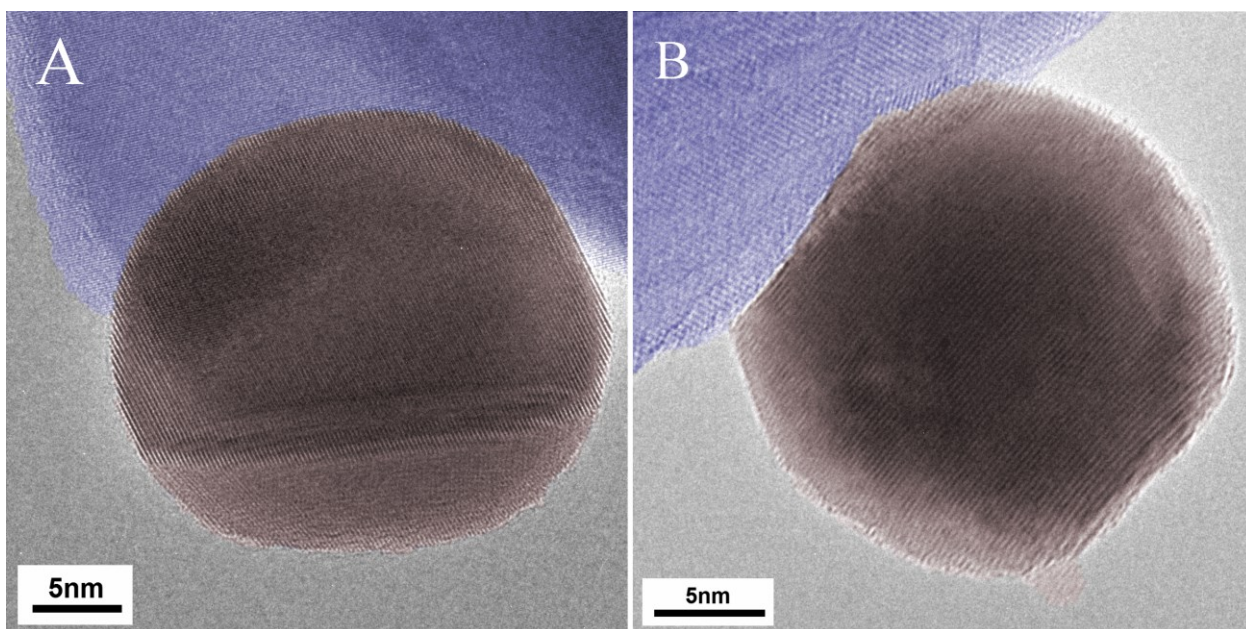


Figure 1. TEM images of Au/Fe₂O₃-PC synthesized by photo-induced decomposition method (A) before and (B) after annealing in O₂ at 300 °C and CO oxidation (CO:O₂=1:2) at 0.3 mbar, 300 °C. Images were colorized in order to highlight the differences between Fe₂O₃ support (blue) and Au NP (red).

3.1.2 XPS characterization.

NAP-XPS provides information about the electronic structure of Au under reaction conditions. Due to carbon contamination on the fresh sample, Au/Fe₂O₃-PC was annealed in O₂ to 300°C to remove the majority of the carbon. Photoelectrons around 160 eV kinetic energy were used to collect the O1s, C1s spectra (Figures 2B and 2C). The spectra collected during annealing in O₂ are presented in Figure 2(i). At the beginning of the annealing process, the C1s spectrum (Figure 2C(i)) shows one intense broad peak at BE of 284.5 eV, which decreases with temperature (not shown). The corresponding O1s spectrum (Figure 2B(i)) consists of three components. The

lowest BE species (529.9 eV) is associated with lattice oxygen of ferric oxide (Fe_2O_3)¹⁶, higher BE species are assigned to the copper oxides/hydroxides (531.6 eV) from the copper mesh^{17,18} and oxygen-containing (hydro)carbons (533.7 eV)¹⁹.

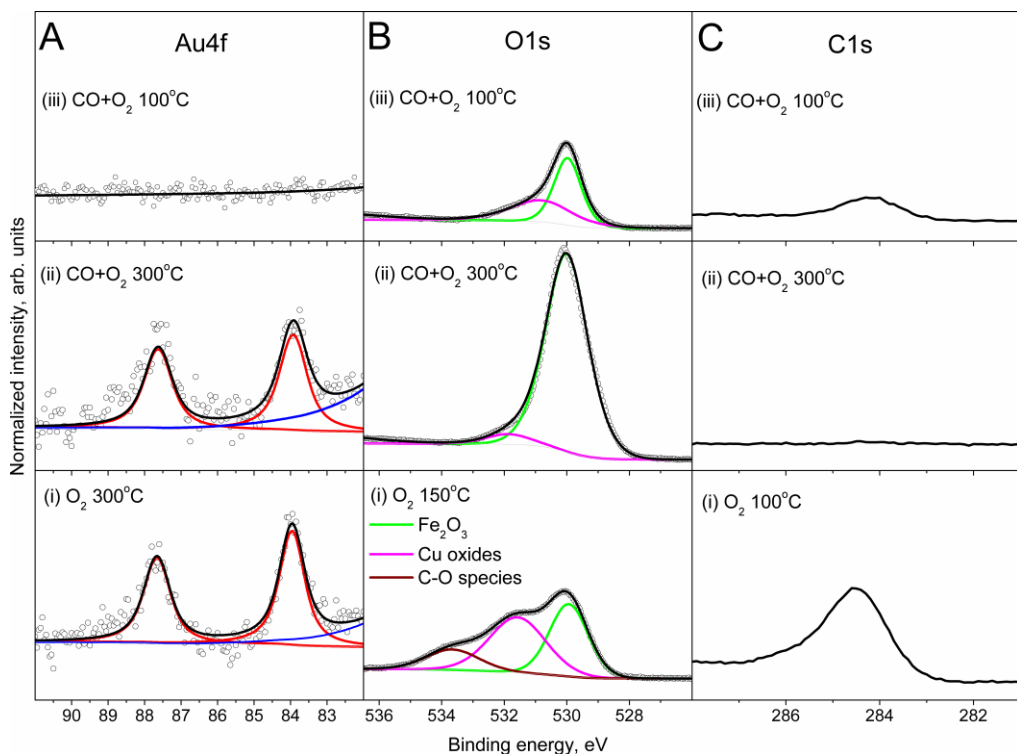


Figure 2. (A) Au4f ($E_{\text{kin}}=900$ eV), (B) O1s ($E_{\text{kin}}=160$ eV) and (C) C1s ($E_{\text{kin}}=160$ eV) XPS spectra of Au/ Fe_2O_3 -PC synthesized by photo-induced decomposition method at 0.3 mbar (i) in O_2 during annealing, (ii) in $\text{CO}+\text{O}_2$ ($\text{CO}:\text{O}_2=1:2$) at 300 °C and (iii) in $\text{CO}+\text{O}_2$ ($\text{CO}:\text{O}_2=1:2$) at 100 °C.

In order to penetrate through the carbonaceous layer, photoelectrons with higher kinetic energy (900 eV) were used for measuring the Au4f spectra (Figure 2A). The Au4f spectrum of Au/ Fe_2O_3 -PC in O_2 at 300 °C (Figure 2A(i)) shows only one sharp peak at a BE of 83.97 eV, assigned to bulk Au in its metal state, in accordance with the accepted Au4f_{7/2} BE value²⁰. Note that the contribution from the neighboring Cu3p_{1/2} peak (blue line in Figure 2A) (BE 77.6 eV)²¹ has to be taken into account for correct fitting.

After annealing, O₂ was substituted by a reaction CO:O₂=1:2 gas mixture at 0.3 mbar, keeping the temperature of Au/Fe₂O₃-PC at 300 °C. The shape of the corresponding Au4f spectrum measured in the reaction gas mixture (Figure 2A(ii)) does not exhibit any changes in comparison with its state during annealing in O₂. The C1s peak totally vanishes (Figure 2C(ii)). The absence of the 533.7 eV peak in the O1s spectrum (Figure 2B(ii)) confirms the carbon removal. The two remaining O1s peaks are assigned to lattice oxygen in Fe₂O₃ (BE 530.0 eV) and copper oxides/hydroxides (BE 531.8 eV). Note, the increase of the intensity of Fe₂O₃ component in the O1s spectrum (Figure 2B(ii)) is a consequence of removing the carbon surface layer; however, the decrease of copper oxide contribution is a result of the presence of CO, which is capable of reducing copper oxides/hydroxides to copper metal. Fe₂O₃ is more stable at low temperature than copper oxides/hydroxides, and cannot be reduced to metal at these temperatures.

Then the sample was cooled down to 100 °C in the reaction gas mixture. Cooling leads to immediate carbon accumulation on the sample surface, as shown in the C1s spectrum (Figure 2C(iii)). The shape of the corresponding O1s spectrum (Figure 2B(iii)) does not change. There is only an intensity decrease, as a consequence of the formation of the overlying carbon layer. As the Au loading is low, the Au4f signal is quite weak, and consequently, after the accumulation of the carbonaceous layer at low temperature, the Au4f signal attenuates so much that it can no longer be detected (Figure 2A(iii)).

3.1.3 Reaction test.

Catalytic activity of Au/Fe₂O₃-PC at 0.3 mbar was below detection limit of the mass-spectrometer, so as-prepared Au/Fe₂O₃-PC was tested in CO oxidation at atmospheric pressure in an oxygen-rich feed (CO:O₂=1:2) (Figure 3). Catalytic activity was monitored at RT, 50 °C and 100 °C but the sample did not produce any CO₂. Subsequent oxidation of the catalyst in 20% O₂

in He was performed at 400 °C for 1 hour, showing the formation of some CO₂ below 350 °C, probably originating from burning of (hydro)carbons from the surface, which may block active sites. However, after the oxidative treatment, the sample became active towards CO oxidation, with CO₂ production already detectible at 50 °C. The activity increased with temperature, showing no sign of deactivation when held at 50 °C and 100 °C. However, when held at 200 °C the production of CO₂ decreased by ca. 28 % over a period of 4 h. The highest amount of CO₂ observed at 200 °C corresponds to a conversion of CO of about 7%. Despite a lot of steps and edges on Au NPs, Au/Fe₂O₃-PC is almost inactive, which shows that only low-coordinated atoms (steps, edges) are not enough to activate Au for CO oxidation.

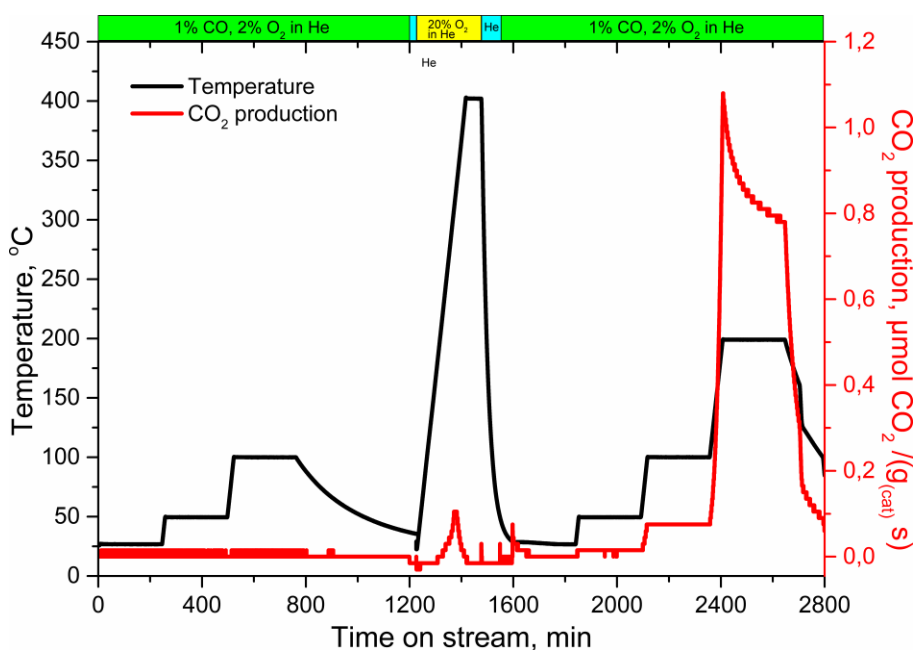


Figure 3. CO₂ production of Au/Fe₂O₃-PC synthesized by photo-induced decomposition method in CO-reactor at 1 bar, CO:O₂=1:2.

3.2 Au/Fe₂O₃-C and Au/TiO₂-DP.

3.2.1 Reaction test.

In contrast to the sample prepared by photo-induced decomposition of the Au-azido-complex, both of the samples synthesized by precipitation methods (Au/Fe₂O₃-C and Au/TiO₂-DP) exhibited high CO₂ yields at 100 °C, without any pretreatment necessary (Figure 4). As shown in Figure 4, CO₂ production increases with increasing CO:O₂ ratio. To exclude the possibility that some background reaction in the chamber was causing this reactivity, the samples were removed from the chamber without interrupting the gas flows. In Figure 4 these moments are apparent by the sharp jumps to infinity in the temperature signal (red line)—i.e. the apparent temperature becomes infinite due to breaking the contact between thermocouple and temperature control stage—occurring at a time on stream of 3 hours in Figure 4A and at 3.7 hour in Figure 4B. It is clear from the corresponding drop in CO₂ signal that the reaction stops immediately once the sample is removed, and restarts once the sample is returned, as seen in Figure 4A.

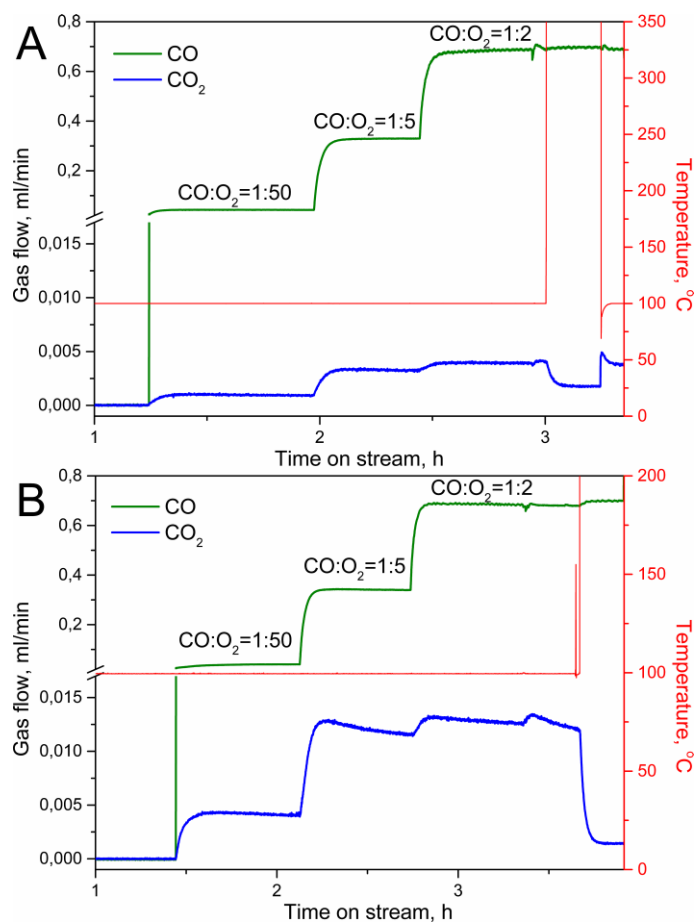


Figure 4. CO₂ production of (A) Au/Fe₂O₃-C synthesized by co-precipitation method and (B) Au/TiO₂-DP synthesized by deposition-precipitation method in NAP-XPS chamber at 0.3 mbar and 100 °C.

Pure oxides (i.e. Fe₂O₃ and TiO₂ without Au NPs) were also tested and did not show any significant activity at low temperature (not shown). This experiment further excludes the contribution of sample holder parts to the activity. Thus, catalytic CO oxidation was found to occur when Au NPs are supported on transition metal oxides. The catalytic performance of Au/Fe₂O₃ and Au/TiO₂-DP samples synthesized by precipitation methods also were tested in a CO-reactor at 1 bar (ESI, Figure S2 and S3) and confirmed the results obtained at 0.3 mbar.

3.2.2 XPS characterization.

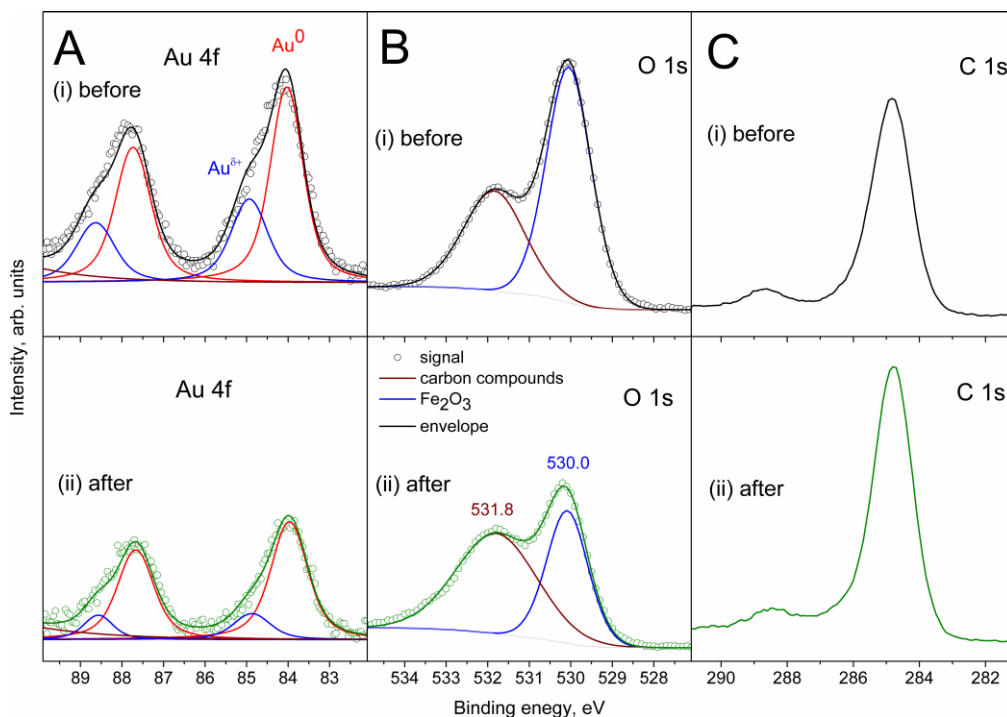


Figure 5. (A) Au4f ($E_{kin}=900$ eV), (B) O1s and (C) C1s ($E_{kin}=160$ eV) XP spectra of Au/Fe₂O₃-C synthesized by co-precipitation method (i) before and (ii) after CO oxidation (CO:O₂=1:2) at 0.3 mbar and 100 °C.

Table 1. Surface composition of Au/Fe₂O₃-C before and after CO oxidation (CO:O₂=1:2) at 0.3 mbar and 100 °C.

	Au ⁰ , %	Au ^{δ+} , %	O, %	C, %	Fe, %
before	0.6	0.3	35.5	50.0	13.6
after	0.4	0.1	29.1	64.6	5.8

To further examine the nature of the Au active sites, NAP-XPS was measured of the Au/Fe₂O₃-C and Au/TiO₂-DP samples. The Au4f core level spectrum of the fresh Au/Fe₂O₃-C, measured in UHV at 100°C before the reaction (Figure 5A(i)), exhibits a main metallic peak at a

BE of 84.0 eV, with a second component shifted to higher BE by 0.9 eV. For proper fitting of Au4f spectra the contribution from Fe 3s peak (BE 93.7 eV)²² has to be taken into account (wine line in Figure 5A). The high-BE Au4f peak is assigned to Au^{δ+}, which can be interpreted as perimeter Au atoms that interact with the metal oxide support via charge transfer^{5,23}.

The corresponding O1s spectrum (Figure 5B(i)) displays two peaks at BE of 530.1 eV and 531.8 eV, respectively. The first peak is assigned to lattice oxygen of Fe₂O₃¹¹ and the second one to oxygen from carbonates and other oxygen-containing (hydro)carbons¹⁹. The presence of carbonates and/or oxygen-containing (hydro)carbons on the surface is confirmed by the very intense C1s spectrum, which consists of a main peak (284.8 eV) and a small peak (C=O bonds or satellite) at 288.5 eV (Figure 5C(i)).

Unfortunately, during the reaction, the sample was partially charging due to the low electrical conductivity of Fe₂O₃ in the presence of an O₂-rich gas mixture at low temperature. Therefore, Au4f, C1s, O1s spectra had to be measured in UHV at 100 °C after the reaction (Figure 5 (bottom panel)) in order to obtain a reliable BE scale.

The C1s peak after the reaction is more intense than before, which indicates carbon accumulation during CO oxidation. Corresponding Au4f, O1s spectra did not change their shapes, only their intensities decreased due to carbon accumulation. Both, Au⁰ and Au^{δ+}, species remained even after reaction, only the Au^{δ+}/Au⁰ ratio decreases from 0.48 to 0.26 after CO oxidation (Table 1). The initial high amount of Au^{δ+} may be because of very small Au NPs (ESI, Figure S4A), which are almost fully cationic. Sintering after CO oxidation (ESI, Figure S4B) results to formation bigger Au NPs, which leads to Au^{δ+}/Au⁰ ratio decreasing.

The Au4f, O1s, C1s XP spectra were also measured for Au/TiO₂-DP (Figure 6). A substantial amount of carbon is present on the surface of untreated Au/TiO₂-DP (Figure 6C (top panel)). In

comparison with the C1s XP spectra of Au/Fe₂O₃-C, the high-BE peak (288.5 eV) is less pronounced; however, the intensities of the main peak (284.9 eV) are comparable. The obtained O1s spectrum consists of two main components: the high-BE component has exactly the same position (531.8 eV) as in case of Au/Fe₂O₃-C, and corresponds to oxygen-containing (hydro)carbons¹⁹; the second O1s peak differs from the Au/Fe₂O₃-C sample, having a BE at 530.5 eV. This BE matches well the position of lattice oxygen of TiO₂²⁴. The asymmetric Au4f spectrum is composed of a metallic peak at a BE of 83.95 eV, a second component shifted to the higher BE by 0.6 eV. The high-BE peak is assigned to an ionic Au species (Au^{δ+})²⁵, which also suggests a strong interaction between the Au NPs and the support material.

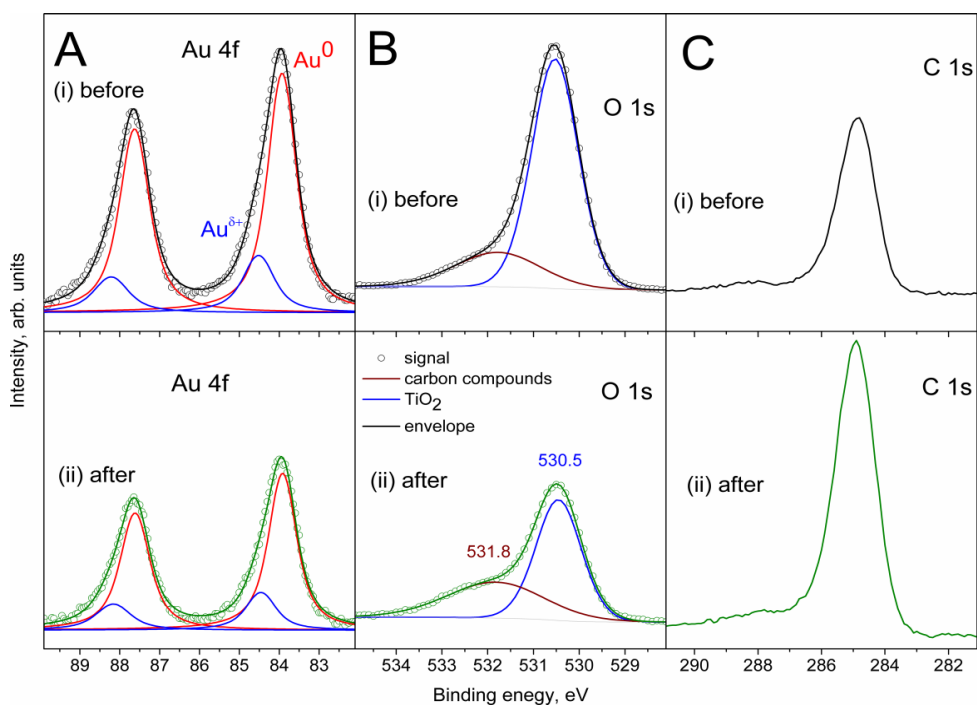


Figure 6. (A) Au4f ($E_{kin}=720$ eV), (B) O1s and (C) C1s ($E_{kin}=160$ eV) XP spectra of Au/TiO₂-DP synthesized by deposition-precipitation method (i) before and (ii) after CO oxidation (CO:O₂=1:2) at 0.3 mbar and 100 °C.

Table 2. Surface composition of Au/TiO₂-DP before and after CO oxidation (CO:O₂=1:2) at 0.3 mbar and 100 °C.

	Au ⁰ , %	Au ^{δ+} , %	O, %	C, %	Ti, %
before	1.1	0.16	48.0	34.7	16.0
after	0.8	0.2	31.7	59.7	7.6

After CO oxidation, both, Au⁰ and Au^{δ+}, species remained as in case of Au/Fe₂O₃-C, but their Au^{δ+}/Au⁰ ratio changed from 0.14 before to 0.26 after reaction (Table 2), which can be due to overlayer formation, because small sintering effect (ESI, Figure S5) should decrease Au^{δ+}/Au⁰ ratio. Also carbon accumulation on support takes place, it leads to an increase of the C1s peak intensity and a decrease of other peak intensities (Figure 6(ii)).

3.2.3 TEM and EELS characterizations.

The combination of XPS and TEM is a powerful approach, since it allows one to correlate electronic structure and morphology. TEM images of the Au/TiO₂-DP sample synthesized by deposition-precipitation method are shown in Figure 7. Au NPs synthesized by deposition precipitation have a mean diameter of 15 nm before and after reaction.

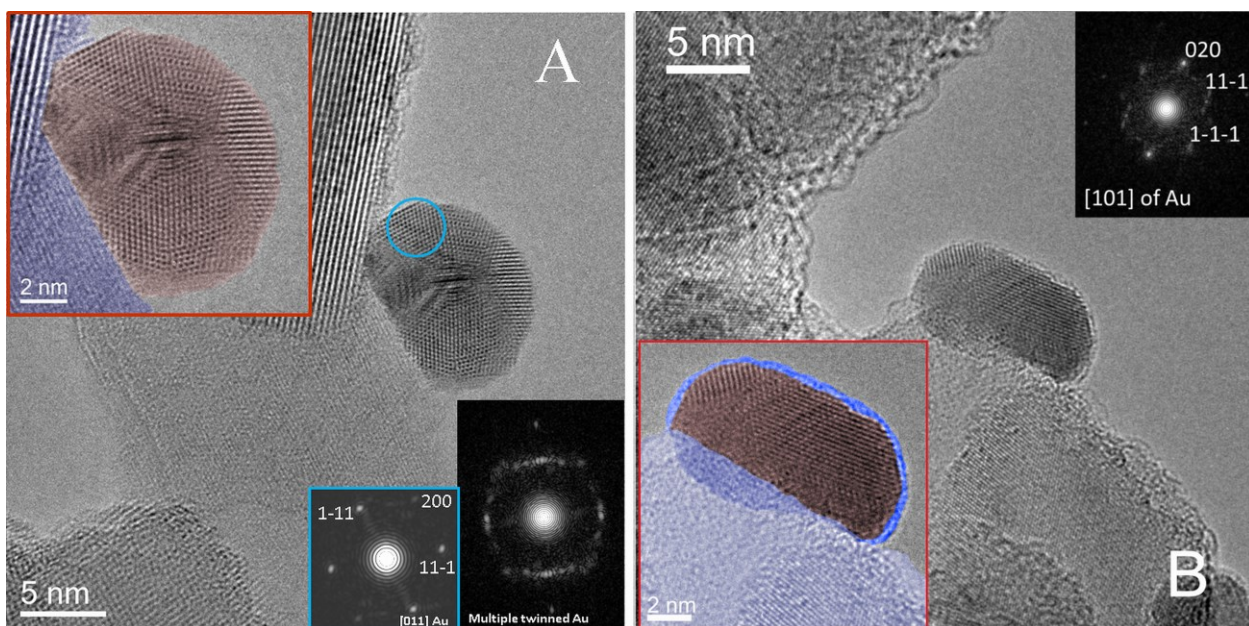


Figure 7. TEM images of Au/TiO₂-DP synthesized by deposition-precipitation method (A) before and (B) after CO oxidation (CO:O₂=1:2) at 0.3 mbar and 100°C. The insets in (A) and (B) represent magnified images and diffraction patterns of the Au nanoparticles. Images were colored in order to highlight the differences between TiO₂ support (pale blue), overlayer (blue) and Au NP (red).

For fresh samples (i.e. prior to use in the CO oxidation reaction), no overgrowth of the support onto the NPs is visible. In contrast, after CO oxidation the Au NPs were covered by a thin layer of support material (blue in Figure 7B). This observation confirms the assumption that a strong metal support interaction (SMSI) is occurring, which may play a key role in the activation mechanism of Au. Similar results were obtained for Au/Fe₂O₃-C sample prepared by coprecipitation method, with overgrowth of the support forming a thin layer over the Au NPs after the CO oxidation reaction; however, the overgrowth layer is not as extensive as in case of Au/TiO₂-DP (ESI, Figure S6).

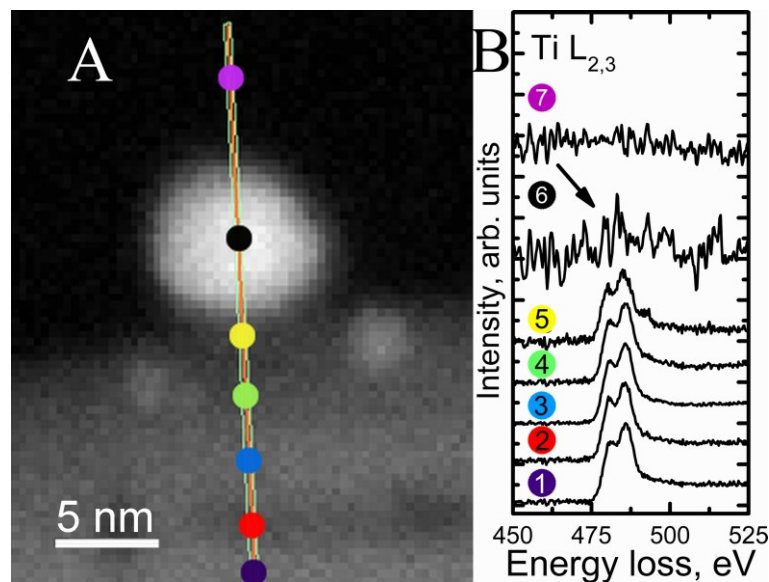


Figure 8. (A) TEM image and (B) corresponding EELS spectra of Au/TiO₂-DP after CO oxidation (CO:O₂=1:2) at 0.3 mbar and 100°C.

We use EELS to clarify the nature of the overgrowth layer after reaction, and confirm whether it originates from the support material. The line scan (Figure 8A) was done and the obtained EELS spectra are presented in Figure 8B. Peaks at energy losses that could be assigned to the Ti L_{2,3}-edges can be observed. The reference TiO₂ EELS spectra (Figure 8B(1)) exhibits much higher intensity as compared to the Au NP (Figure 8B(6)). Although the Ti signal on the Au NP is quite weak, the presence of this peak indicates a TiO_x overgrowth on the Au NP. Only a weak and featureless signal from the C K-edge is obtained (ESI, Figure S7) from a larger region. Therefore, the EELS measurements confirm that the overlayer arises from overgrowth of the oxide support onto the Au NPs, and that there is indeed an SMSI between Au NPs and these transition metal oxides.

3.2.4 Kinetic measurements.

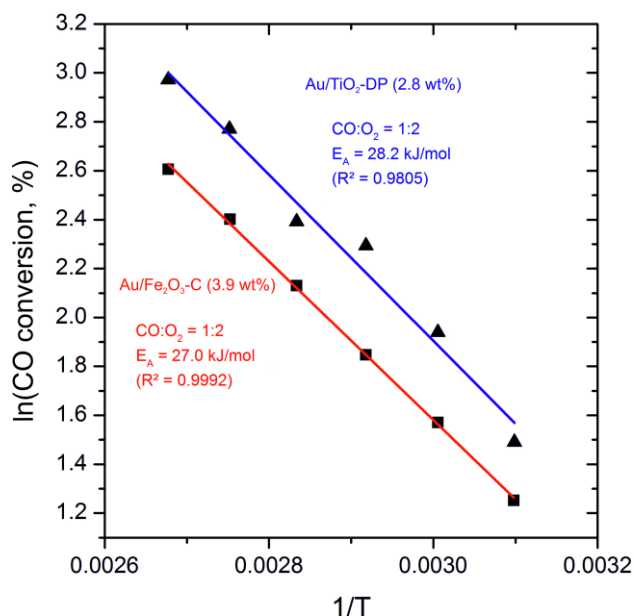


Figure 9. Arrhenius plot of Au/TiO₂-DP (blue line) and Au/Fe₂O₃-C (red line).

In order to estimate activation energies for CO oxidation at ambient pressure on Au/Fe₂O₃-C and Au/TiO₂-DP, samples were placed in a CO oxidation reactor. CO conversion was measured at six different temperatures without any pre-treatment, yielding the Arrhenius plot shown in Figure 9. While the Au/TiO₂-DP sample shows higher conversion rates than Au/Fe₂O₃-C at all temperatures, the activation energies of both samples are similar (27.0 kJ/mol and 28.3 kJ/mol for Au/Fe₂O₃-C and Au/TiO₂-DP, respectively). Thus one may conclude that Au/TiO₂-DP had more active sites than Au/Fe₂O₃-C, but that CO oxidation on both systems may occur via same mechanisms.

Comparison of the activities at 373 K yields about 7 $\mu\text{mol CO}_2 \text{ g}_{[\text{Au}]}^{-1} \text{ s}^{-1}$ for photo-chemically prepared Au/Fe₂O₃-PC after oxidative pre-treatment (673 K) and 20 $\mu\text{mol CO}_2 \text{ g}_{[\text{Au}]}^{-1} \text{ s}^{-1}$ Au/Fe₂O₃-C by co-precipitation without any pre-treatment. The most active sample was

Au/TiO₂-DP, with a yield of 35 $\mu\text{mol CO}_2 \text{ g}_{[\text{Au}]}^{-1} \text{ s}^{-1}$. The most important results are summarized in Table 3.

Table 3. Main finding of presented study.

	Au/Fe ₂ O ₃ -PC	Au/Fe ₂ O ₃ -C	Au/TiO ₂ -DP
BE difference between Au ^{δ^+} and Au ⁰ , eV	-	+0.9	+0.6
degree of wetting	low	high	high
overlayer formation	no	low	high
activation energy, kJ/mol	-	27.0	28.3
CO ₂ rate, $\mu\text{mol CO}_2 \text{ g}_{[\text{Au}]}^{-1} \text{ s}^{-1}$	<7	20	35

4. DISCUSSION

Our experiments reveal that activity of Au on transition metal oxides, such as Fe₂O₃ and TiO₂, depends on the method of synthesis. Samples prepared by the precipitation method showed high CO₂ production at low temperature, independent of the metal oxide. It is known that the method of synthesis is crucial for controlling the activity of a catalyst²⁶. Au NPs synthesized by photo-induced decomposition do not possess any significant catalytic activity because of minimal interaction with the metal oxide support. Most preparation methods produce large NPs that are inactive for CO oxidation, but deposition precipitation provides good control over particle size. The preparation of Au/TiO₂ by deposition precipitation has been studied in detail by Moreau et al.²⁷ and they outline that the method allows one to control many experimental parameters (concentration, temperature, pH, time, etc.).

As is apparent from the XPS results, two Au species are formed on the active catalysts. TEM images of these samples reveal the formation of an extended interface between the Au NPs and

the oxide support. Therefore, it is possible that the $\text{Au}^{\delta+}$ component seen in the XP spectra is due to a species formed by a strong interaction between the surface Au atoms and overgrowth layer from the oxide supports. In the literature there is much debate concerning the nature of the active site for Au-based catalysts. Various factors, such as quantum size effects²⁸, low coordinated atoms, surface ions and the support interactions⁶, have been proposed to influence the activity of Au. Some authors consider metallic gold¹⁸ to be the active site, while others suggest positive ($\delta+$)²⁹ or negative ($\delta-$)³⁰ low-charged gold or oxidized (1+, 3+) states³¹. Some years ago Bond and Thomson⁵ proposed a model where Au atoms at the interface between Au and the oxide are the active oxidation centers; however, they focus on a mechanistic debate, while the electronic structure of active Au remained unclear.

Some groups link the activity of Au to the transition from metallic to non-metallic particles.^{28,32} Small unsupported clusters showed significant shifts in XP spectra, the shifts are correlated with coordination numbers of the Au atoms in the clusters.³³ Theory predicts that small Au NPs are very reactive, because of high concentration of low-coordinated Au atoms.³⁴ However, the transition take place at particles with 100 atoms (diameter of <2 nm).³⁵ This is valid for free flying particles and clusters not interacting with their support, but these conditions do not represent the reality for cases where Au NPs strongly interact with supports of different kinds.³⁶ Nevertheless, both opinions are right within their respectively different conditions: ones ignore the support, while the others ignore possible absence of support effect. We have shown that both cases can be realized within polycrystalline materials and we have identified the induced strong support interaction through the method of synthesis as the controlling factor.

Our present findings suggest that, on the particulate form of active catalyst, gold is present in both cationic and metallic forms, where the atoms at the triple-phase boundary are assumed to be

of cationic nature. These results are in a good agreement with previous works of Costello et al.³⁷ and Kung et al.²³, where a chemical model that involves an ensemble of metallic Au atoms and Au cations with hydroxyl ligands has been suggested.

It must also be noted that XP spectra of Au NPs are markedly affected by final-state effects, and furthermore, BE of the Au⁰ is size-dependent for small nanoparticles³⁸. In our case, because of rather large Au NPs and simultaneously observed shifted and unshifted Au species, at homogeneous particle sizes the contribution from final-state effects to BE shift can be excluded, so the positive BE shifts are the result of the interaction between Au and the oxide support. The similarity in the high-BE shift values of Au/TiO₂ and Au/Fe₂O₃ synthesized by precipitation methods suggests the same origin for both samples, i.e. SMSI. The small difference in chemical shift arises due to different interaction strengths (charge transfer) between Au and two oxides. The high-BE shift value (0.6 eV) for Au/TiO₂-DP correlates well with Chusuei's work.²⁵ Yang and Wu³⁹ showed that the high-BE shift is caused by the interaction of gold with oxygen vacancies and not by final-state effects; there is no evidence for Au³⁺ presence at the interface. DFT calculations also identify the importance of Au-oxide interaction in CO oxidation.⁴⁰

The obtained TEM images reliably show that the formation of an overgrowth layer occurs only after the reaction. The overgrowth layer from the support is evidence of a SMSI. Furthermore, the higher CO₂ production rate of Au/TiO₂-DP than Au/Fe₂O₃-C may be explained by different interaction strengths between Au and the support. Indeed, Grunwald et al.⁴¹ showed higher activity of Au/TiO₂ in comparison with Au/ZrO₂ even though the particle sizes were identical. They believe that the support affects the ability of Au to dissociate oxygen. Also Au-based catalysts supported on 'non-reducible' metal oxide supports (Au/Al₂O₃) have considerably less activity than those supported on 'reducible' metal oxide supports (Au/Fe₂O₃, Au/TiO₂).⁴² Au-

assisted Mars-van Krevelen mechanism for reducible support^{43,44} may be the origin of the overgrowth layer.

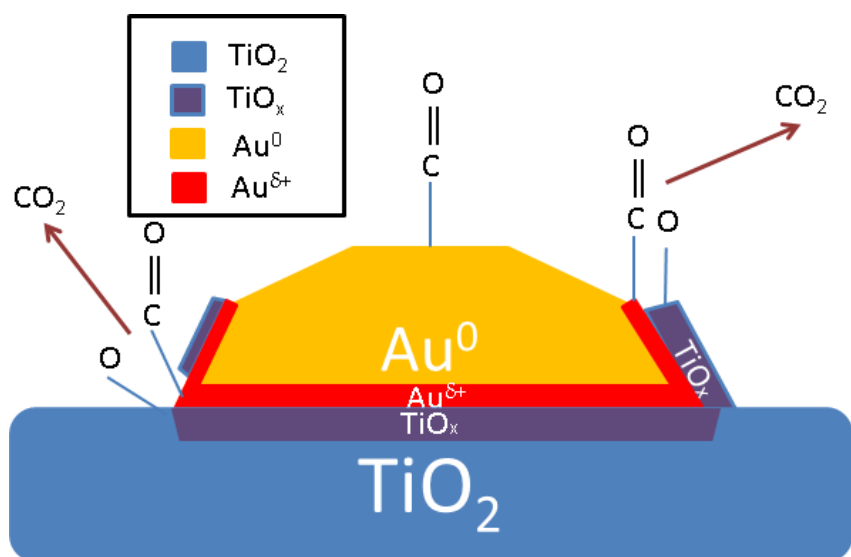
The activation energy values calculated from Arrhenius plots and specific surface area measurements (S_{BET}) of our samples, Au/Fe₂O₃-C and Au/TiO₂-DP, prepared by precipitation methods are shown in Table 4 together with a comparison with data from the literature. Despite the similarity of activation energy values and sizable difference in specific surface area, 27.0 kJ/mol and 28.2 kJ/mol, 206.8 m²/g and 54.8 m²/g for Au/Fe₂O₃-C and Au/TiO₂-DP, respectively, the activity of Au/TiO₂-DP is much higher, which suggests higher numbers of active sites on the surface. More defects (for instance twins or symmetrical intergrowth of crystals, low-coordinated atoms) are evident for the Au particles supported on titania due to lattice mismatch. Because of the existence of numerous defects on the surface of active samples, SMSI also enables stabilization of defects (edges, twins, kinks, etc.).

Table 4. Activation energies and specific surface area of Au/Fe₂O₃ and Au/TiO₂ prepared by different methods.

Catalysts	Preparation method	S_{BET} [m ² /g]	E_a [kJ/mol]	Ref.
Au/Fe ₂ O ₃	DP		29	45
	DP		35	46
	DP with phosphine		21	47
	co-precipitation	206.8	27.0	This work
	co-precipitation	73		1
	co-precipitation	45		48
	DP	196.1		49
Au/TiO ₂	DP		27	50
	DP with phosphine		12	47

	impregnation		21	45
	impregnation		29	51
	DP	54.8	28.2	This work
	DP	44		48
	DP	81.8		52
	colloidal deposition	47		53

Our results agree well with the proposed reaction pathway (Scheme 1) for the CO oxidation reaction over supported Au catalysts, as described by Schubert et al.⁴⁵ Oxygen adsorbs in large quantities on reducible metal oxides and then migrates to the Au NPs. Dissociation of the mobile oxygen is suggested to take place at the metal–support interface, after which it reacts with CO adsorbed on the gold and/or at the interface. Therefore, the formation of an overlayer increases the interface area, which leads to increases in CO₂ yield. An increase in interface area can be achieved by decreasing the particle size, which also leads to a significant increase of CO₂ production.^{28,42}



Scheme 1. Suggested CO oxidation pathway on transition metal oxides.

5. CONCLUSIONS

The results presented here indicate that the Au NPs on transition metal oxides show high catalytic activity, which depends on the method of preparation, and can be associated with the formation of positively charged Au species. Indeed, only the samples prepared by precipitation methods showed significant CO conversion at low temperature. XPS revealed the presence of two Au species (Au^0 and $\text{Au}^{\delta+}$) on the surface of active Au/TiO₂-DP and Au/Fe₂O₃-C samples. The energy shift of the $\text{Au}^{\delta+}$ peak, relative to bulk gold (Au^0), depends on the support, and is 0.6 eV and 0.9 eV to higher BE for Au/TiO₂-DP and Au/Fe₂O₃-C, respectively. TEM images indicate the formation of overlayers on Au particles. EELS spectra confirm that the overlayers consist of support material—i.e. transition metal oxide overlayers on top of the Au NPs.

Our results suggest a mechanism of Au activation via Strong Metal Support Interaction (SMSI), and assume that the support overlayer has a strong influence on the electronic structure of the gold through charge transfer and stabilization of low-coordinated Au atoms. Therefore, we suggest that SMSI plays key role in Au activation and is more important than size reduction.

ASSOCIATED CONTENT

Supporting Information.

Synthesis methods, particle size distributions, CO₂ production of Au/Fe₂O₃-C and Au/TiO₂-DP in CO-reactor at ambient pressure, TEM monitoring of Au/Fe₂O₃-C, TEM image and EELS spectrum of Au/TiO₂-DP, large area TEM images and fitting parameters of Au4f_{7/2} and O1s spectra of all samples. This material is available free of charge via the Internet at <http://pubs.acs.org>.

Corresponding Author

*E-mail: klyushin@fhi-berlin.mpg.de

ACKNOWLEDGMENT

We thank HZB for the allocation of synchrotron radiation beamtime, Maike Hashagen (Fritz-Haber-Institute der Max-Planck Society, Berlin) for BET measurements.

REFERENCES

- (1) Haruta, M.; Yamada, N.; Kobayashi, T.; Iijima, S. *J. Catal.* **1989**, *115*, 301-309.
- (2) Min, B. K.; Friend, C. M. *Chem. Rev.* **2007**, *107*, 2709-2724.
- (3) Hutchings G. J.; Edwards J. K. *Application of gold nanoparticles in catalysis*; Roy L. J., Wilcoxon J. P., Eds.; Frontiers of Nanoscience; Elsevier, Amsterdam, 2012, Vol. 3, pp. 249–293.
- (4) Meyer R.; Lemire C.; Shaikhutdinov Sh. K.; Freund H.-J. *Gold Bull.* **2004**, *37*, 72-124.
- (5) Bond, G. C.; Thompson, D. T. *Gold Bull.* **2000**, *33*, 41–51.
- (6) Klyushin, A. Yu.; Youngmi, Y.; Xie, Z.; Arrigo, R.; Hävecker, M.; Bukhtiyarov, A. V.; Prosvirin, I. P.; Bukhtiyarov, V. I.; Knop-Gericke, A.; Schlögl, R. *Top. Catal.* **2016**, *59*, 469-477.
- (7) Lu, J.-L.; Gao, H.-J.; Shaikhudinov, S.; Freund, H.-J. *Catal. Lett.* **2007**, *114*, 8-16
- (8) Boccuzzi, F.; Chiorino, A.; Manzoli, M. *Surf. Sci.* **2000**, *454–456*, 942-946.

- (9) Tripathi, A. K.; Kamble, V. S.; Gupta, N. M. *J. Catal.* **1999**, *187*, 332–342.
- (10) Starr, D.E.; Shaikhutdinov, Sh.K.; Freund, H.-J. *Top. Catal.* **2005**, *36*, 33-41.
- (11) Valden, M.; Pak, S.; Lai, X.; Goodman, D. W. *Catal. Lett.* **1998**, *56*, 7-10.
- (12) Glaspell, G.; Fuoco, L.; El-Shall, M. S. *J. Phys. Chem. B* **2005**, *109*, 17350-17355.
- (13) Li, W.-C.; Comotti, M.; Schüth, F. *J. Catal.* **2006**, *237*, 190-196.
- (14) Schwartz, V.; Mullins, D. R.; Yan, W.; Chen, B.; Dai, S.; Overbury, S.H. *J. Phys. Chem. B* **2004**, *108*, 15782-15790.
- (15) Bluhm, H.; Hävecker, M.; Knop-Gericke, A.; Kiskinova, M.; Schlögl, R.; Salmeron, M. *MRS Bull.* **2007**, *32*, 1022-1030.
- (16) Grosvenor, A. P.; Kobe, B. A.; McIntyre, N. S. *Surf. Sci.* **2004**, *572*, 217–227.
- (17) Ertl, G.; Hierl, R.; Knozinger, H.; Thiele, N.; Urbach, H. P. *Appl. Surf. Sci.* **1980**, *5*, 49-64.
- (18) Cano, E.; Torres, C. L.; Bastidas, J. M. *Mater. Corros.* **2001**, *52*, 667-676.
- (19) Schaefer, A.; Ragazzon, D.; Wittstock, A.; Walle, L. E.; Borg, A.; Bäumer, M.; Sandell, A. *J. Phys. Chem C* **2012**, *116*, 4564-4571.
- (20) Canning, N. D. S.; Outka, D.; Madix, R. J. *Surf. Sci.* **1984**, *141*, 240–254.
- (21) Mansour, A. N. *Surf. Sci. Spectra* **1994**, *3*, 202-210.
- (22) Allen, G. C.; Harris, S. J.; Jutson, J. A.; Dyke, J. M. *Appl. Surf. Sci.* **1989**, *37*, 111-134.

- (23) Kung, H. H.; Kung, M. C.; Costello, C. K. *J. Catal.* **2003**, *216*, 425-432.
- (24) Stefanov, P.; Shipochka, M.; Stefchev, P.; Raicheva, Z.; Lazarova, V.; Spassov, L. *J. Phys. Conf. Ser.* **2008**, *100*, No. 012039.
- (25) Chusuei, C.; Lai, X.; Luo, K.; Goodman, D. W. *Top. Catal.* **2001**, *14*, 71-83.
- (26) Zanella, R.; Delannoy, L.; Louis, C. *Appl. Catal. A Gen.* **2005**, *291*, 62-72.
- (27) Moreau, F.; Bond, G. C.; Taylor, A. O. *J. Catal.* **2005**, *231*, 105-114.
- (28) Valden, M.; Lai, X.; Goodman, D. W. *Science* **1998**, *281*, 1647-1650.
- (29) Boccuzzi, F.; Chiorino, A.; Manzoli, M.; Lu, P.; Akita, T.; Ichikawa, S.; Haruta, M. *J. Catal.* **2001**, *202*, 256-267.
- (30) Chen M. S.; Goodman D. W. *Science* **2004**, *306*, 252-255.
- (31) Minicò, S.; Scirè, S.; Crisafulli, C.; Visco, A. M.; Galvagno S. *Catal. Lett.* **1997**, *47*, 273-276.
- (32) Vinod, C.P.; Kulkarni, G.U.; Rao, C.N.R. *Chem. Phys. Lett.* **1998**, *289*, 329-333.
- (33) DiCenzo, S. B.; Berry, S. D.; Hartford, E. H. *Phys. Rev. B* **1988**, *38*, 8465-8468.
- (34) Lopez, N.; Janssens, T.V.W; Clausen, B.S.; Xu, Y.; Mavrikakis, M.; Bligaard, T.; Nørskov, J.K. *J. Catal.* **2004**, *223*, 232-235
- (35) Lee, S.-T.; Apai, G.; Mason, M. G.; Benbow, R.; Hurych Z. *Phys. Rev. B* **1981**, *23*, 505-508.

- (36) Di Valentin, C.; Scagnelli, A.; Pacchioni, G.; Risse, T.; Freund, H.-J. *Surf. Sci.* **2006**, *600*, 2434-2442
- (37) Costello, C. K.; Yang, J. H.; Law, H. Y.; Wang, Y.; Lin, J.-N.; Marks, L. D.; Kung, M. C.; Kung, H. H.. *Appl. Catal. A Gen.* **2003**, *243*, 15-24.
- (38) Mason, M. G. *Phys. Rev. B* **1983**, *27*, 748-762.
- (39) Yang, Z.; Wu, R. *Phys. Rev. B* **2003**, *67*, No. 081403.
- (40) Liu, Z.-P.; Gong, X.-Q.; Kohanoff, J.; Sanchez, C.; Hu P. *Phys. Rev. Lett.* **2003**, *91*, No. 266102.
- (41) Grunwaldt, J.-D.; Kiener, C.; Wögerbauer, C.; Baiker, A. *J. Catal.* **1999**, *181*, 223-232.
- (42) Schubert, M. M.; Hackenberg, S.; van Veen, A. C.; Muhler, M.; Plzak, V.; Behm, R. J. *J. Catal.* **2001**, *197*, 113-122.
- (43) Widmann, D.; Behm, R. J. *Angew. Chem. Int. Ed.* **2011**, *50*, 10241-10245.
- (44) Lohrenscheit, M.; Hess, C. *ChemCatChem* **2016**, *8*, 523-525.
- (45) Schubert, M. M.; Hackenberg, S.; van Veen, A. C.; Muhler, M.; Plzak, V.; Behm, R. J. *J. Catal.* **2001**, *197*, 113-122.
- (46) Haruta, M.; Tsubota, S.; Kobayashi, T.; Kageyama, H.; Genet, M. J.; Delmon, B. *J. Catal.* **1993**, *144*, 175-192.
- (47) Kozlov, A. I.; Kozlova, A. P.; Liu, H., Iwasawa, Y. *Appl. Catal. A* **1999**, *182*, 9-28.

- (48) Solsona, B. E.; Garcia, T.; Jones, C.; Taylor, S. H.; Carley, A. F.; Hutchings, G. J. *Appl. Catal. A-Gen.* **2006**, *312*, 67–76.
- (49) Liu, R.; Gao, N.; Zhen, F.; Zhang, Y.; Mei, L.; Zeng, X. *Chem. Eng. J.* **2013**, *225*, 245-253.
- (50) Haruta, M. *Catal. Today* **1997**, *36*, 153-166.
- (51) Bollinger, M. A.; Vannice, M. A. *Appl. Catal. B* **1996**, *8*, 417-443.
- (52) Liu, J.; Si, R.; Zheng, H.; Geng, H.; Dai, W.; Chen, X.; Fu, X. *Catal. Commun.* **2012**, *26*, 136–139
- (53) Widmann, D.; Liu, Y.; Schüth, F.; Behm, R. J. *J. Catal.* **2010**, *276*, 292–305.